# Depth-resolved cathodoluminescence study of zinc oxide nanorods catalytically grown on p-type 4H-SiC

Nargis Bano, I Hussain, Omer Nour, Magnus Willander, Qamar Ul Wahab,
Anne Henry, H S Kwack, D Le Si Dang



Original Publication:

Nargis Bano, I Hussain, Omer Nour, Magnus Willander, Qamar Ul Wahab, Anne Henry, H S Kwack, D Le Si Dang, Depth-resolved cathodoluminescence study of zinc oxide nanorods catalytically grown on p-type 4H-SiC, 2010, JOURNAL OF LUMINESCENCE, (130), 6, 963-968.
http://dx.doi.org/10.1016/j.jlumin.2010.01.006

# Depth-resolved cathodoluminescence study of zinc oxide nanorods catalytically grown on p-type 4H-SiC

**N. Bano, I. Hussain, O. Nur and M. Willander**

Department of Science and Technology, Campus Norrköping, Linköping University, SE-60174 Norrköping, Sweden

**Q. Wahab and A. Henry**

Department of Physics Chemistry and Biology, Linköping University, SE-58183 Linköping, Sweden

**H. S. Kwack and D Le Si Dang**

CEA-CNRS Group 'Nanophysique et Semiconducteurs', Institut N´eel, CNRS and Universit´e Joseph Fourier, F-38042 Grenoble, France

## ABSTRACT

Optical properties of ZnO nanorods (NRs) grown by vapour-liquid-solid (VLS) technique on 4H-p-SiC substrates were probed by cathodoluminescence (CL) measurements at room temperature and at 5 K complemented with electroluminescence. At room temperature the CL spectra for defect related emission intensity was enhanced with the electron beam penetration depth. We observed a variation in defect related green emission along the nanorod axis. This indicates a relatively poor structural quality near the interface between ZnO NRs and p-SiC substrate. We associate the green emission with oxygen vacancies. Analysis of the low-temperature (5 K) emission spectra in the UV region suggests that the synthesized nanorods contain shallow donors and acceptors.

## 1. INTRODUCTION

Zinc oxide (ZnO) with wurtzite structure has a large direct band gap around 3.4 eV and a large exciton binding energy (60 meV), which offers efficient excitonic emission at room temperature and above, is an ideal material for optoelectronic application. Due to these properties, ZnO has been a focus of active research for the past several years [1,2]. In optoelectronics ZnO possesses potential for various applications such as light-emitting diodes and lasers [3, 4]. However the stable and reproducible p-type doping in ZnO is still a problem, which is hindering the realization of a ZnO p-n homo-junction diode [5]. The hetero-junction devices often show less efficiency than homo-junction devices because an energy barrier is created at the junction, which decreases carriers injection efficiency. This problem can be solved by making many nanosized junctions, because the carrier injection rate can be increased in nanojunctions, leading to better efficiency [6]. ZnO possesses a rich family of nanostructures such as nanorods (NRs), nanowires (NWs) and nanoneedles, as some examples [7]. All such nanostructures have been successfully synthesized and have attracted interest because they can be used as building blocks for future optoelectronic devices. These nanostructures have many advantages among which large surface to volume ratio, good crystal quality and unique photonic properties [8, 9]. So far, among these structures, the NRs of ZnO are grown with relatively better crystalline quality with lower defect density compared to bulk and thin films due to their small footprint and the release of strain and stress due to the relaxing large surface area to volume ratio. At the same time, both ends of ZnO NRs are extremely smooth, making them perfect mirror planes and vertical NRs are like natural waveguide cavities for making the emitted light to travel to the top of the device, also minimizing partial leakage and thus enhancing the light extraction efficiency from the surface [10]. In recent years, ZnO based nanostructures have been

studied intensively for applications to UV and visible light emitting and field emission devices [11]. Photoluminescence (PL) is considered as an important tool for optical characteristics of ZnO-nanostructures [12]. ZnO has two main emission bands in its room temperature PL spectrum; these are a sharp UV band and deep band emission (DBE) or green emission due to deep defect states in the band gap [12, 13]. Although much research on the origin of the deep band emission has been published, no consensus was reached. ZnO can exhibit different emissions in the visible range including violet, blue, green, yellow, and orange-red, which are associated with intrinsic as well as extrinsic defects [2, 13]. The free carrier concentration, doping compensation, minority carrier lifetime, and luminescence efficiency are directly or indirectly related to the defects [14]. The causes for the formation of these defects (intrinsic or extrinsic) and their spatial distribution are still controversial. ZnO based optical/electrical devices depend upon the defect chemistry and the understanding of the optical/electrical properties, both of which are the subject of recent theoretical and experimental studies. The spatial resolution for the PL is limited due to the diffraction limit and poor signal to noise ratio. In most of the cases the PL is taken from a group of NRs, which makes it difficult to investigate local or individual characteristics of NRs under illuminations [15]. For the detailed emission information and to explain the origin of specific emission from specific small area, even from individual nanostructures, a probe with high spatial and spectral resolutions is preferable. In this respect, depth resolved cathodoluminescence (CL) spectroscopy is performed, which records luminescence after creating electron-hole pairs by high energy electron bombardment and provide more information with its high spatial resolution, especially for nanostructures. Depth resolved cathodoluminescence spectroscopy is capable of probing the band gap, and the deep level defect features as a function of their positions in the band gap at different locations in the

nanorod, enabling a wide range of information. Furthermore the information on the physical origin and growth dependence of the electrically active defects can also be extracted [16].

In this study we report the use of cathodoluminescence (CL) as a local luminescence characterization tool for ZnO NRs to obtain detailed luminescence information and especially to verify the origin of specific emissions from ZnO NRs and distribution of radiative defects along vertical ZnO NRs. Green luminescence band that originates from defects is related to the electrical/optical characteristics of nanostructures, because defects are responsible for a wide modification of electrical/optical properties of ZnO [17]. Many future nanoscale systems can benefit from the optical properties of nanostructures. So it is important to obtain the detailed information about luminescence and verify the origin of specific emissions from ZnO NRs. Depth resolved cathodoluminescence spectroscopy technique involves an incident electron beam of an energy that produces free electron-hole pair recombination across the bandgap or between deep levels and the band edges. The CL penetration depth increases with increase in the beam energy, as determined by the energy-range relationships for energy loss within a solid [18, 19]. CL signals from different depth positions within the band gap of the material can be excited and thus an average depth distribution of luminescence can be determined. The acceleration voltage for this study was varied from 1 to 30 kV, which corresponds to a maximum penetration depth of 0.04 – 2.16 μm as calculated from the Kanaya-Okayama model [19].

**EXPERIMENTAL DETAIL:**

ZnO NRs were grown on a p-type SiC thin film. The p-type SiC film was grown by conventional CVD technique on n-SiC commercial substrate [20]. The acceptor concentration in the p-SiC thin film was around $5x10^{18}$ $cm^{-3}$ and the thickness was around 1 μm. The ZnO NRs

were grown by the vapour-liquid-solid (VLS) technique [13]. First we cover a small portion of the p-SiC substrate for defining ohmic contacts on p-SiC. After that a layer of 2-5 nm thick Au film was deposited on the p-type SiC. Then ZnO (99.9%) powder was mixed with graphite (99.9%) powder with 1:1 ratio. This mixed powder was then vaporized. The substrate coated with Au was placed at a certain distance from a boat containing the mixture of ZnO and graphite powder and then growth was initiated at 890 $^{o}$C and continued for 30 min. After growth the samples were processed to fabricate light emitting diodes (LEDs) to perform complementary electroluminescence (EL). For the ohmic contact on the substrate first we etched small portion of the p-SiC, which was covered before the growth of the ZnO NRs. After that a thin layer of Ni/Al was used. The contact was annealed at 900 $^{o}$C for 3 min in Ar atmosphere. Prior the ohmic contacts on the ZnO NRs an insulating PMMA layer was deposited between the NRs. To ensure that no PMMA was on the top of the NRs, oxygen plasma cleaning was performed prior to the contact metal deposition. Then Al contacts of diameter 0.5 mm were evaporated onto a group of NRs. The grown structure was characterized by scanning electron microscope (SEM), cathodoluminescence (CL) and electroluminescence (EL). The CL spectra of our samples were measured with varying acceleration voltages (1-30 keV), which allow probing the sample and optical emissions at different depths along ZnO NRs. However, the depth of the "generation volume" by electron beam depends on the materials and the electron beam energy. Monochromatic CL imaging obtained for selected emission wavelengths using a single channel photomultiplier tube (PMT) and spectral analysis of the CL measured for samples using the nitrogen cooled charge-coupled device (CCD) camera. The luminescence is collected by a parabolic mirror and dispersed by a 0.55 meter monochromator equipped with a 600 $mm^{-1}$ grating. We used two modes of excitation and these are as follows: (1) the scan mode for which

the electron beam is scanned within a certain area during the CL measurement; (2) the spot mode for which the electron beam is kept fixed, and we used the spot size of 3 (beam diameter is 50 nm). From this condition of the CL system, we measured the CL spectra for the samples at both room temperature (RT) and low temperature (5 K).

The EL measurements of the ZnO NRs-based hetero-junction LED was carried out using a photo multiplier detector under dc-bias condition at room temperature. The light was collected from the topside of the device.

**RESULTS AND DISCUSSION**

The ZnO NRs grown were found to be vertically aligned and distributed uniformly. The typical length of the nanorods varies in the range 1.9-2.2 μm while the widths of NRs vary between 0.4 and 0.6 μm as shown in the SEM image in Figure 1. The inset in Figure 1 shows the ZnO NRs after insulator deposition followed by etching.

Figure 2 show curves of energy loss per unit depth, dE/dx, as a function of depth into the target material (ZnO) for 20 kV and 30 kV accelerated voltages. These curves present a polynomial fit to the Everhart-Hoff depth dose relation [18], which takes into account the density and the average atomic weight. In order to understand the emission property from ZnO NRs, it is necessary to clarify the effect of electron beam conditions on the CL measurement. Accelerating voltage is considered as a main parameter is affecting the electron beam [21]. Therefore, the depth dependent CL spectra were investigated.

Figure 3 shows the dependence of CL spectra on the accelerating voltage for ZnO NRs at a temperature of 5 K. The CL intensity is displayed in a logarithmic scale to emphasize the bands of weaker intensities. The beam current is set to 56 pA. The CL spectra exhibit ultraviolet near

band edge (NBE) emission peak at 369 nm, which is related to the direct recombination of electron beam-generated charge carriers (excitonic emission), a deep band emission (DBE) centered at 510 nm and a red emission around 600-800 nm. No luminescence is observed for an accelerating voltage of 1.0 kV, luminescence bands started to appear slightly above 2.0 kV and the intensity increased with the accelerating voltage. The edge emission peak was found to split into a variety of narrow peaks due to bound-exciton recombinations and electron recombination from allowed bands to shallow levels. A narrow bound-exciton peak at 369 nm and two longer wavelength peaks, at 374.44 nm (3.325 eV) and 382.72 nm (3.253 eV), are shown in Fig. 3. Given that the phonon replica features near the ZnO band edge that corresponds to energies of 70-72 meV, consistent with the 580-590 $cm^{-1}$ $E_1$(LO) longitudinal optical phonon in bulk ZnO, we correlate the peak at 382.72 nm to phonon replicas of the peak at 374.44 nm[22].

To gain greater insight into the defect chemistry, we measured CL spectra at room temperature (RT). Figure 4a shows the RT-CL spectra at different accelerating voltages (2-30 kV). The number of excited carriers is considered to be in proportion to accelerating voltage. The beam current is kept at 56 pA as described previously. The CL spectra exhibit NBE emission at 380 nm, which is related to the direct recombination of photon-generated charge carriers (excitonic emission) a green band centered at 521 nm and a red emission centered at 750 nm . The peaks shift at RT is due to difference in band gap at 5 K and at RT. It is noted that the whole CL spectra are red shifted because the sample was heated by the electron bombardment.

The penetration depth ($U_0$) which is related to electron-hole pair creation rate, varies with incident electron accelerating voltages such that $U_0$=0.04, 0.1, 0.4, 1.14 and 2.16 μm for $V_b$ = 2, 5, 10, 20 and 30 kV, respectively. An electron acceleration voltage of 20 kV corresponds to 1μm of penetration depth [18]. The RT-CL spectra exhibit orders of magnitude lower NBE and high

DBE which shows that defect concentrations is varying in orders of magnitude with depth on a nanometer scale. The CL emission intensities of the NBE emission, DBE and red as a function of the penetration depth are shown in Fig.4b. The band-edge and green emission show distinct differences in depth dependence but the red emission illustrates weak depth dependence. For the penetration depth in the range of 0-0.4 μm, the NBE intensity is higher relative to the NBE intensity at the upper interface and tends to reach saturation. For the penetration depth between 1 -2.21 μm the green emission intensity is higher than the NBE intensity. By increasing the accelerating voltage, the electron beam is expected to penetrate deeper into the NRs and excites more electron-hole pairs near and below the penetration depth. In this way, more and more emission centers will be excited by the electron bombardment. It is found in bulk and thin films of ZnO that the UV emission from ZnO can be internally reabsorbed by the crystal itself within a 1μm range [23]. However, this reabsorbed UV emission can excite defect states in the material resulting in DBE. Thus, part of the UV emission may contribute to the enhancement of the DBE [24]. The differences and variations in the size of the nanostructures also contribute to the emission intensities. A luminescence spectrum usually represents the optical characteristics of all the nanostructures inside the probing area, due to inhomogeneities among the nanostructures it may be considered as an average luminescence [25]. Remarkably, the ratio of the band edge to the DBE intensity, which is used as a criterion for the nano-rods quality, decreases with penetration depth within the whole length of our NRs. As a result from Fig. 4b, it is concluded that there are more deep defects at the root of ZnO NRs. Willander et al. demonstrated that ZnO NRs have more structural defects at the interface of the ZnO NRs and the substrate than the top, by HR-TEM study [7]. Chien-Lin et al. [26] reported that the NBE and DBE are emitted separately from two opposite halves of the nano-rods. The CL spectroscopy gives in depth

information about radiative defects step by step using this technique it is concluded that ZnO NRs have more radiative defects at the interface.

The actual signal in CL spectrum originates from different depth positions depending on the electron beam accelerating voltage ($V_b$), therefore the CL signal in the material can be excited at different depth positions, and thus a rough depth distribution of luminescence is determined. However the excitation power ($I_bV_b$), which is proportional to the carrier generation rate, was controlled by keeping the accelerating voltage ($V_b$) constant while varying the beam current ($I_b$). The beam current ($I_b$) was regulated by the spot size. At a constant voltage ($V_b$), the beam current ($I_b$) increases with increasing spot size. Careful analysis of excitation power dependence of the CL spectra allows us to determine the depth distribution of the luminescence centers [27]. Figure 5a shows the dependence of the CL spectra on the beam current. The accelerating voltage was fixed at 10 kV and current varies from 4.2 - 240 pA. The CL intensity of NBE emission is increasing relative to the DBE and the intensity of NBE emission is saturated at a current of 240 pA. Figure 5b shows the intensity of the NBE as a function of the electron beam current. From Figure 5b, the NBE increases linearly and the saturated cathodoluminescence intensity is observed at the electron beam current of 240 pA (also see Fig. 5a.

We also measured a CL spectrum from an area containing no ZnO, but at the SiC. The CL spectra of SiC have very weak emission at 390 nm and 540 nm but the CL spectra of ZnO NRs show stronger emissions at 380 nm and DBE (420-720 nm) centered at 521 nm as shown in Fig. 6. Fig. 6 confirms that most of the emission is originating from ZnO NRs, and the SiC has a minute contribution to the emission.

The corresponding RT-EL spectrum for forward injection current is shown in Figure 7. This EL spectrum shows two peaks. These are DBE at 525 nm and a red emission at 683 nm. The peak positions in the EL spectra are different than in the CL spectra because the sample was heated by the electron bombardment during CL measurements.

In the literature, there is still controversy about the origin of the luminescence centers observed in ZnO material [12]. Several groups have reported that different defect centers in ZnO are responsible for the DBE and red emissions. Leiter et. al. observed a broad, DBE centered at 2.45 eV and assigned it to the oxygen vacancy (Vo) [28]. Using theoretical considerations, the DBE observed at 2.38 eV has been attributed to the oxygen antisite ($O_{Zn}$) [29], other candidates are zinc vacancies [30], interstitial zinc ($Zn_i$) [31], and Cu impurities [31]. In our case, the green emission should be attributed to the point defects mentioned above. The variation in the green emission peak position is attributed to different relative contributions from, e.g. $V_O$, $V_{Zn}$, $O_{Zn}$ and Cu related defects caused by fluctuations in the growth conditions for different growth methods [13]. In the CL and EL spectra, the DBE has a peak at 521 ±0.04 nm we can say that this is due to $V_O$ in the ZnO nanorods due to which green light is emitted which contribute to the white light emitted from the device. The red emission is attributed to interstitial zinc ($Zn_i$) [12]. Surface or bulk oxygen vacancies are often cited as the origin of n-type conduction in ZnO, which has been questioned in recent years [32]. Oxygen vacancies, zinc interstitials, or hydrogen are thought to be responsible for the n-type conduction. Although the DBE is not directly related to those shallow donors, the density of defects giving DBE can be proportional to that of shallow donors if they have similar origins such as different charging states of oxygen vacancies [25]. This would explain the relation between higher carrier density and green luminescence observed because the carrier density for our hetrojunction diode is $1.4\times10^{18}cm^{-3}$. Detailed analysis

indicates that the DBE band in ZnO NRs is due to both isolated oxygen vacancies (short-wavelength side) and donor-acceptor pairs (long-wavelength side) with an oxygen vacancy ($V_O$) as the donor [33, 34]. At room temperature-CL spectra DBE at 521 nm arises from electron transitions from the energy level of isolated vacancies to the valence band. Analysis of the low-temperature edge-emission spectra in the UV region suggests that the synthesized nanorods contain shallow donors and acceptors. As follows from results of the peak at 369 nm, is due to the radiative recombination of neutral donor-bound excitons [35]. The most likely neutral donors are the native defect species $Zn_i$ and $V_O$, due to local zinc enrichment in the crystal lattice of ZnO [25]. To fully understand the origin of the correlation between luminescence and transport characteristics, more systematic investigation of samples are necessary. The inhomogeneities observed among ZnO nanostructures can be attributed to fluctuations during growth and formation of the nanostructures. Investigation of inhomogeneities among ZnO nanostructures grown by different methods can shed some light on the fundamental growth mechanisms and their improvements.

In summary, we have shown that depth resolved cathodoluminescence can provide information about the quality of ZnO NRs, the role of defects and optical characterization of ZnO NRs with high spatial resolution. The room temperature CL spectra of ZnO NRs exhibit NBE emission as well as strong defect related green and red emission peaks. In the CL spectra, the defect related green emission was increased with the increase of the electron beam penetration depth due to the increase of defect concentration at the interface and due to the conversion of self-absorbed UV emission. This indicates a rather poor structural quality close to the p-SiC substrate. The CL spectra at temperature 5 K in the UV region suggest that the ZnO NRs contain shallow donors and acceptors.

**Reference:**


[1] C.-Y. Chang, F.-C. Tsao, C.-J. Pan, G.-C. Chi, H.-T. Wang, J.-J. Chen, F. Ren, D. P. Norton, S. J. Pearton, K.-H. Chen, and L.-C. Chen, Appl. Phys. Lett. **88**, 173503 (2006).

[2] C. Klingshirn, Phys. Stat. Sol. b **244**, 3027 (2007).

[3] A. Tsukazaki, A. Ohtomo, T. Onuma, M. Ohtani, T. Makino, M. Sumiya, K. Ohtani, S. F. Chichibu, S. Fuke, Y. Segawa, H. Ohno, H. Koinuma, M. Kawasaki, Nat. Mater. **4**, 42 (2005).

[4] D. M. Bagnall, Y. F. Chen, Z. Zhu, T. Yao, S. Koyama, M. Y. Shen, T. Goto, Appl. Phys. Lett. **70**, 2230 (1997).

[5] S. K Hong, T. Hanada, H. Makino, Y. Chen, H. J. Ko, and T. Yao, Appl. Phys. Lett. **78**, 21 (2001).

[6] W. I. Park, and G. C. Yi, Adv. Mater. **16**, 1 (2004).

[7] M. Willander, O. Nur, Q. X. Zhao, L. L. Yang, M. Lorenz, B. Q. Cao, J. Zúñiga Pérez, C Czekalla, G Zimmermann, and M. Grundmann, A. Bakin, A. Behrends, M. Al- Suleiman, A. El-Shaer, A. Che Mofor, B. Postels and A. Waag, N. Boukos and A. Travlos H. S. Kwack, J. Guinard, and D. Le Si Dang, Nanotechnol. Top. Rev., in press (2009).

[8] A. Kolmakov, M. Moskovits, Annu. Rev. Mater. Res. **34**, 151-180 (2004).

[9] Z. L. Wang, J. Phys. Condens. Matter. **16**, R 829-R858 (2004).

[10] E. Lai,W. Kim and P. Yang, J. *Nano Research* **2,** 1,123-128, (2008).

[11] T-T Cuong , F. Matthew and R. P. Matthew, Nanotechnology **19**, 415606 (2008).

[12] A. B. Djurišić, Y. H. Leung, Small **2**, 944 ( 2006).

[13] T. M. Børseth, B. G. Svensson, A. Y. Kuznetsov, P. Klason, Q. X. Zhao, M. Willander, Appl. Phys. Lett. **89**, 262112 (2006).

[14] Hadia Noor, P. Klason, O. Nur, Q. Wahab, M. Asghar, and M. Willander, J. Appl. Phys. **105**, 123510 (2009).

[15] M. O. Young, M. L. Kyung, P. H. Kyung, K. Yongsun, Y. H. Ahn, P. Ji-Yong and L. Soonil, Nano Lett. **7**, 3681 (2007**)**.

[16] L. J. Brillson J. Vac. Sci. Technol. B **19**, 5 (2001).

[17] L. Schmidt-Mende, J. L. MacManus-Driscoll, Mater. Today **10**, 40 ( 2007).

[18] T. E. Everhart and P. H. Hoff, J. Appl. Phys. **42**, 5837 (1971)

[19] K. Kanaya and S. Okayamal, J. Phys. D **5**, 43 (1972).

[20] A. Henry, J. Hassan, J. P. Bergman, C. Hallin, E. Janzen, Chem. Vap. Deposition **12**, 475 (2006).

[21] B. Dierre, X. L. Yuan, N. Ohashi, and T. Sekiguchi, J. Appl. Phys. **103**, 083551 (2008).

[22] L. J. Brillson, H. L. Mosbacker, D. L. Doutt, Y. Dong, Z.-Q. Fang, D. C. Look, G. Cantwell, J. Zhang, J. J. Song, Superlat.Microstruct. **45**, 206-213(2009)

[23] H. Yoshikawa and S. Adachi, Jpn. J. Appl. Phys. **36**, 6237 (1997).

[24] X. Zhiyan, O. Morihro, I. Masayoshi, I. Tadashi, H. Gui, N. Yoichiro, A. Toru and M. Hidenori, J. Surf. Sci. Nanotechnol. **7**, 358 (2009).

[25] M. O. Young, M. L. Kyung, P. H. Kyung, K. Yongsun, Y. H. Ahn, P. Ji-Yong and L. Soonil, Nano Lett. **7**, 3681 (2007**)**.

[26] K. Chien-Lin, W. Ruey-Chi, H. Jow-Lay, L. Chuan-Pu, L. Yi-Feng, W. Cheng-Yu and C. Hung-Chin Nanotechnology **19**, 285703 (2008).

[27] X. Li and J. J. Coleman Appl. Phys. Lett. **70**, 27 (1997).

[28] F. H. Leiter, H. Alves, D. Pfisterer, N. G. Romanov, D. M. Hofmann, and B. K. Meyer, Physica B **340**, 201 (2003).

[29] B. Lin, Z. Fu, and Y. Jia, Appl. Phys. Lett. **79**, 943 (2001).

[30] Y. W. Heo ,D. P. Norton and S. J. Pearton, J. Appl. Phys. **98**, 073502 (2005).

[31] N. Y. Garces, L. Wang, L. Bai, N. N. C. Giles, L. E. Halliburton, G. Cantwell, Appl. Phys. Lett. **81**, 622 (2002).

[32] L. Schmidt-Mende, J. L. MacManus-Driscoll, Mater. Today **10**, 40 (2007).

[33] A. N. Gruzintsev, A. N. Red'kin, Z. I. Makovei, V. I. Kozlovskii and Ya. K. Skasyrskii, Inorg. Mater. **42**, 872 (2006).

[34] A. N. Gruzintsev and E. E. Yakimov, Neorg. Mater. **41**, 828 (2005).

[35] Q. X. Zhao, M. Willander, R. E. Morjan, Q-H. Hu and E. E. B. Campbell, Appl. Phys. Lett., **83**, 165 (2003).

**Figure captions:**

**Figure 1:** SEM image of as grown ZnO NRs on p-type epitaxial layer on 4H-SiC substrate. Inset shows the SEM image after spin coating and followed by soft backing.

**Figure 2:** The energy loss characteristic dE/dx versus depth curves for two energies.

**Figure 3:** Depth dependent CL spectra of ZnO NRs taken at a spot size of 50 nm at temperature of 5 K.

**Figure 4: (a)** Depth dependent CL spectra of ZnO NRs taken at a spot size of 50 nm at room temperature, and **(b)** The emission intensity (right axis) of the NBE, green band and red as well as the ratio of NBE and green bands (left axis) as a function of penetration depth.

**Figure 5: (a)** RT-CL spectra taken at a series of electron beam current values while maintaining a constant beam voltage ($V_b$=10 kV), with the beam spot size in the range of 2–100 nm, and **(b)** The peak intensity of the NBE, green band and red as a function of electron beam current.

**Figure 6:** Comparison of the CL emission spectra from ZnO NRs and nearby area without ZnO NRs (4H-SiC area).

**Figure 7:** Room temperature EL spectra of ZnO NRs.

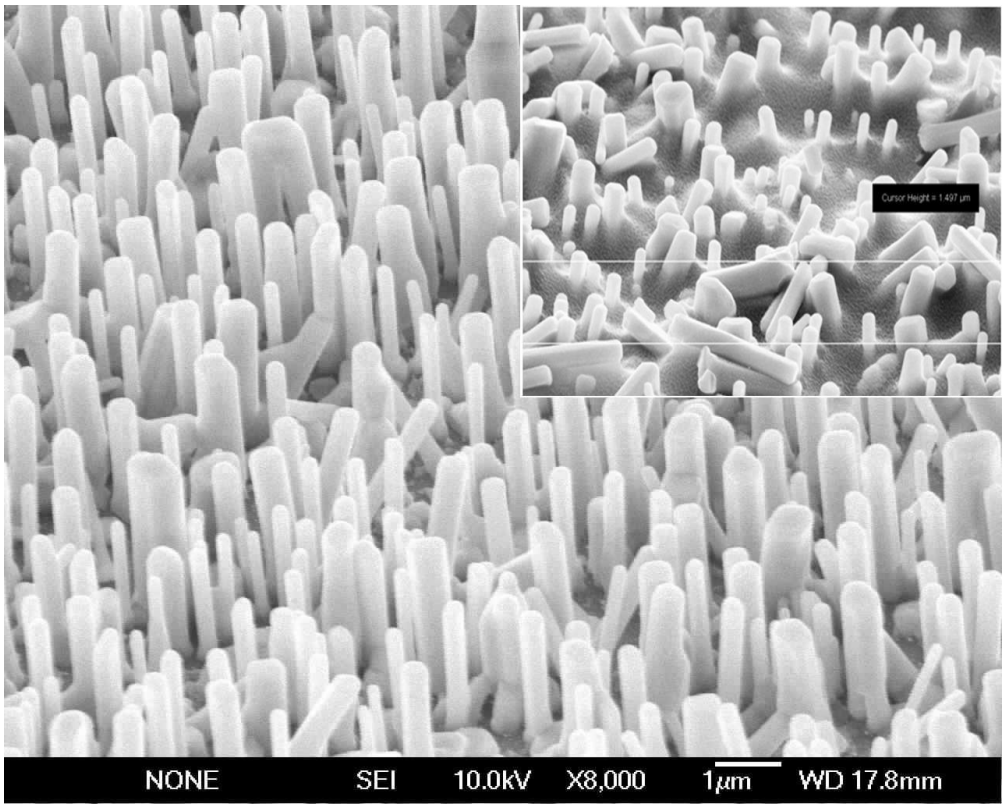


**Figure 1**

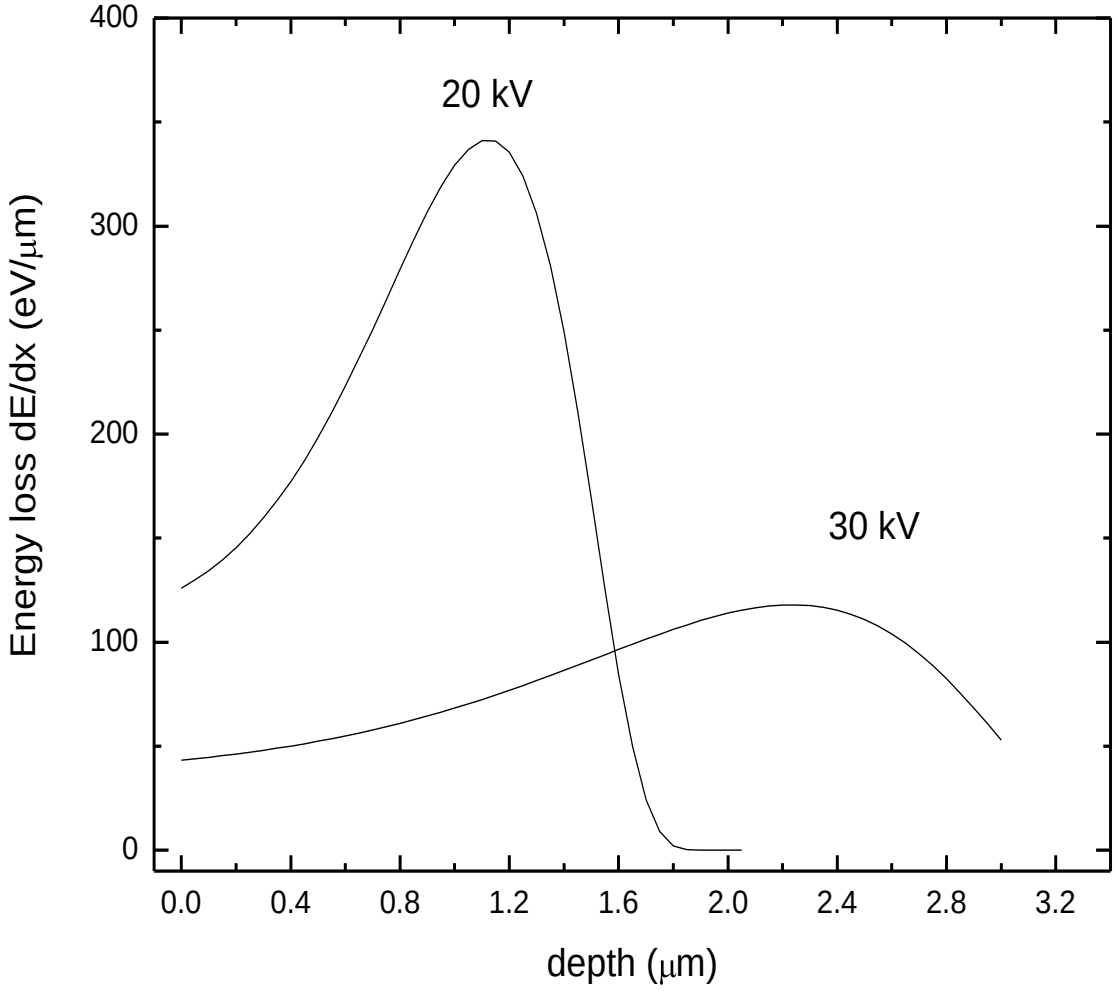
400
300
200
100
0
20 kV
30 kV
Energy loss dE/dx (eV/μm)
0.0
0.4
0.8
1.2
1.6
2.0
2.4
2.8
3.2
depth (μm)

**Figure 2**

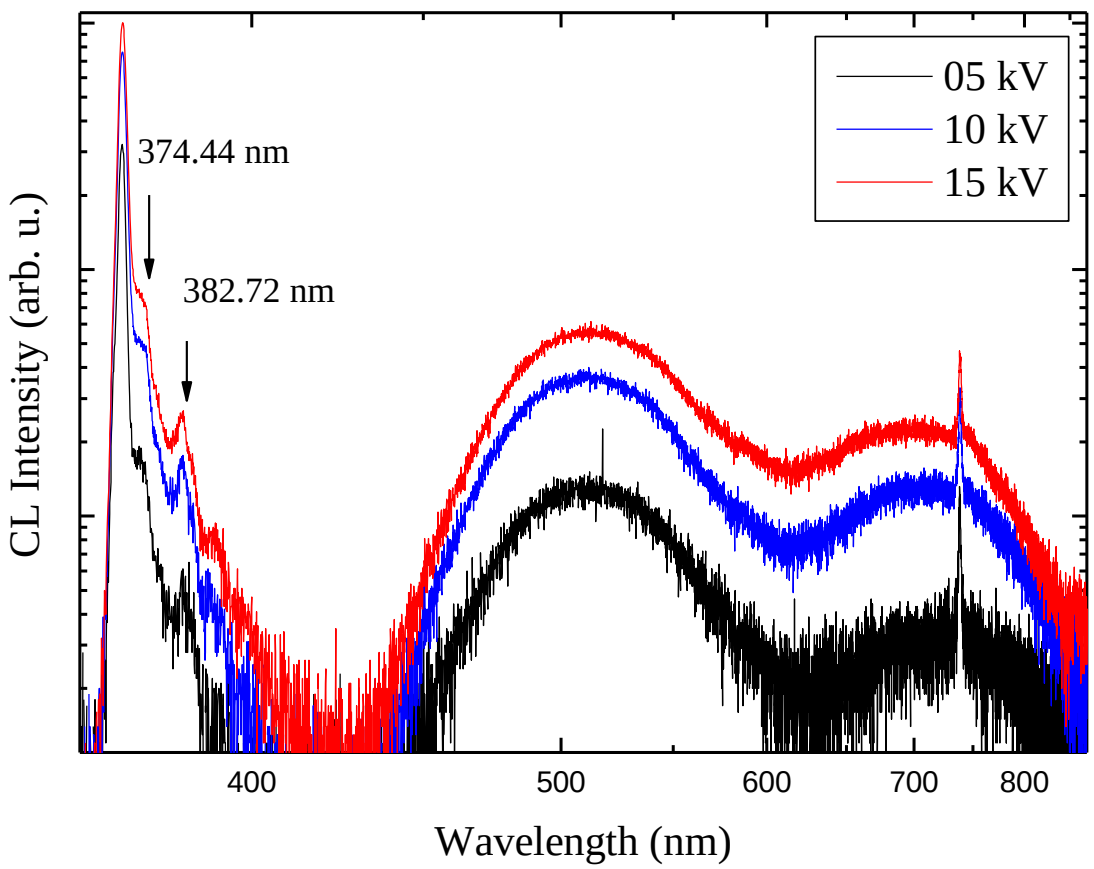
05 kV
10 kV
15 kV
374.44 nm
382.72 nm
CL Intensity (arb. u.)
400
500
600
700
800
Wavelength (nm)

**Figure 3**

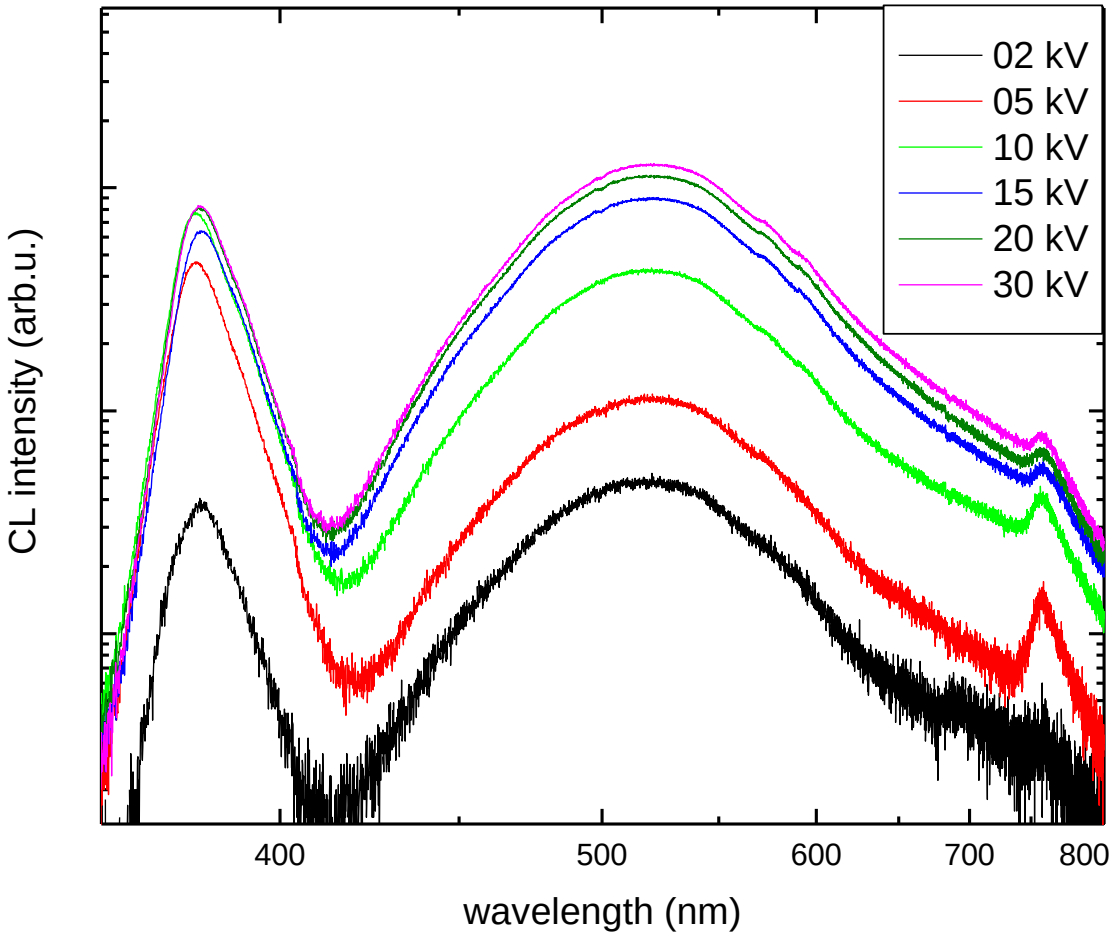
02 kV
05 kV
10 kV
15 kV
20 kV
30 kV
CL intensity (arb.u.)
400
500
600
700
800
wavelength (nm)

**Figure 4 (a)**

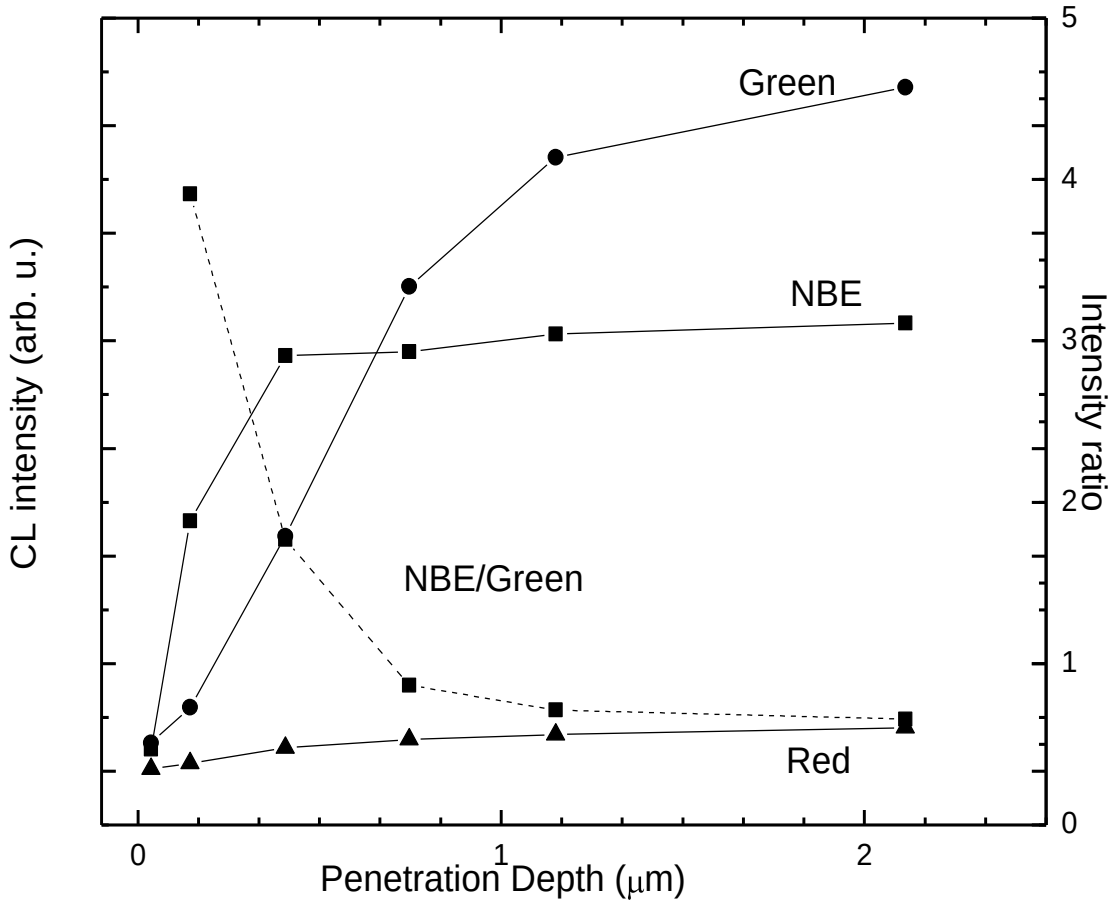
Green
NBE
NBE/Green
Red
CL intensity (arb. u.)
Intensity ratio
Penetration Depth (μm)
0
1
2
0
1
2
3
4
5

**Figure 4 (b)**

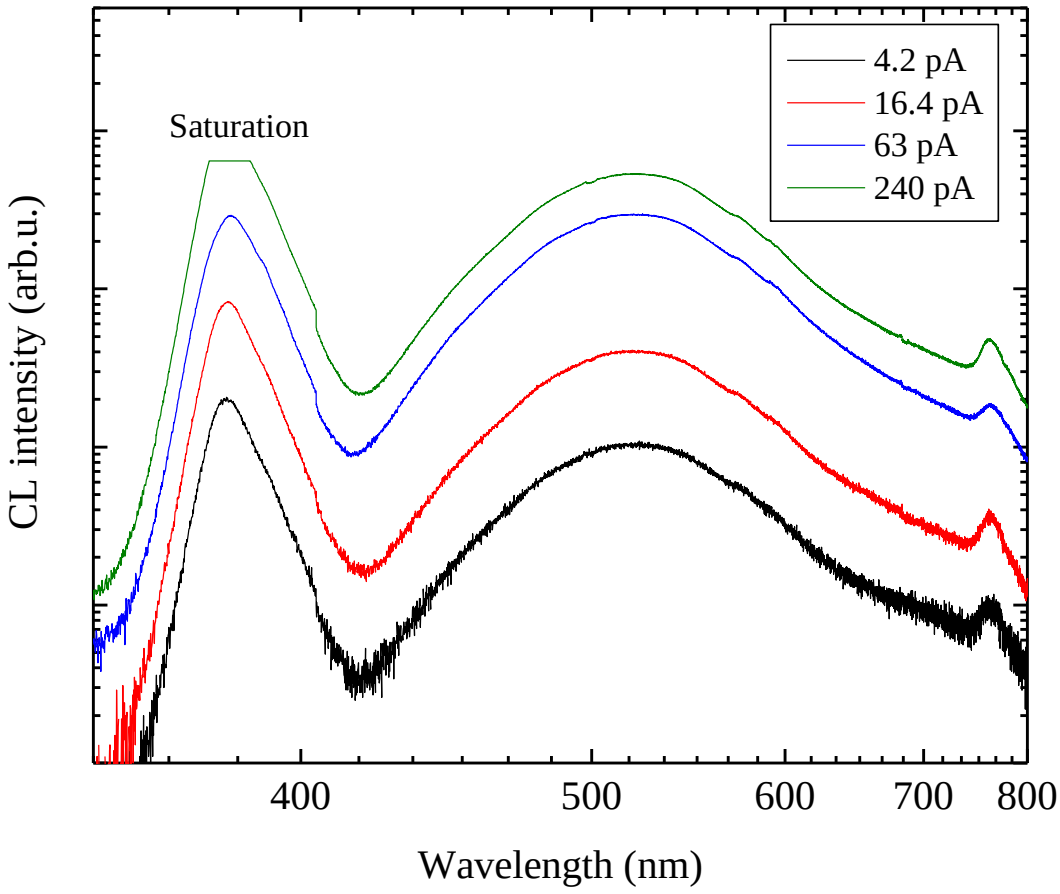
Saturation
4.2 pA
16.4 pA
63 pA
240 pA
CL intensity (arb.u.)
400
500
600
700
800
Wavelength (nm)

**Figure 5(a)**

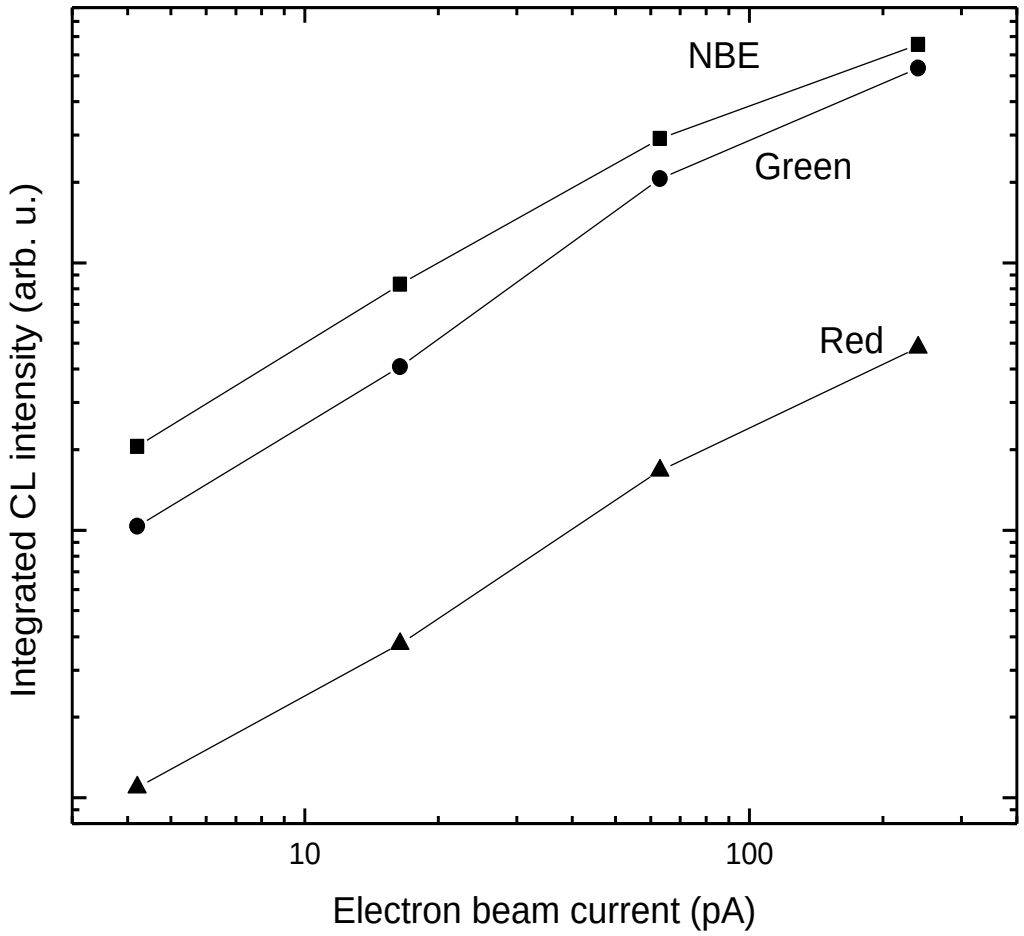
NBE
Green
Red
Integrated CL intensity (arb. u.)
10
100
Electron beam current (pA)

**Figure 5(b)**

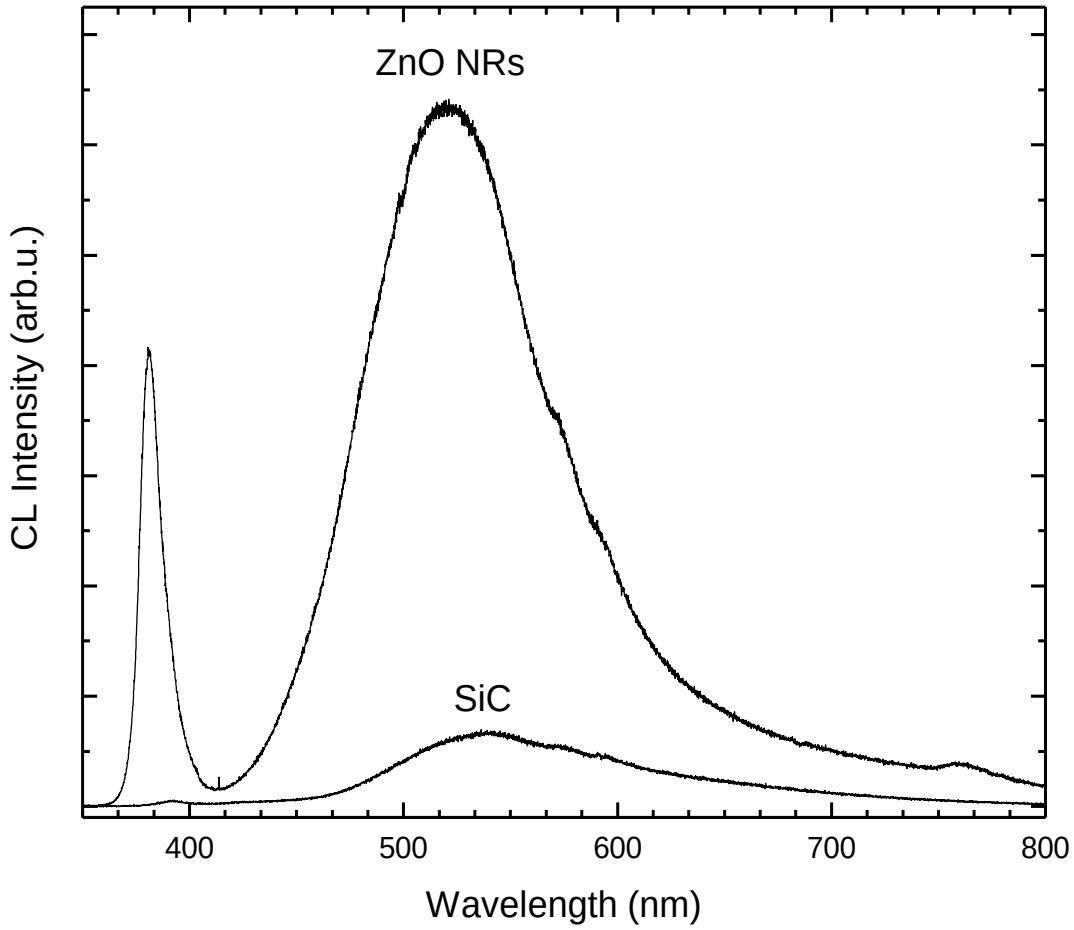
ZnO NRs
SiC
CL Intensity (arb.u.)
400
500
600
700
800
Wavelength (nm)

**Figure 6**

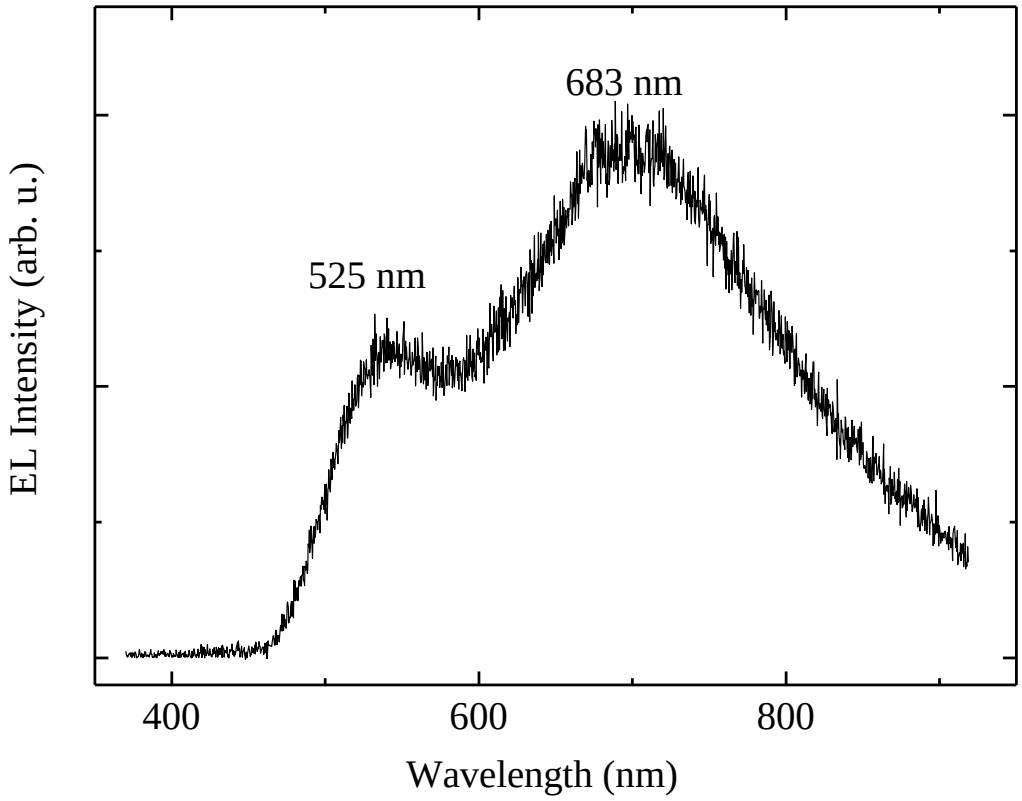


**Figure 7**